International Journal of Heat and Mass Transfer 55 (2012) 325–335

Contents lists available at SciVerse ScienceDirect

International Journal of Heat and Mass Transfer

journal homepage: www.elsevier.com/locate/ijhmt

Electromagnetic field effects on transport through porous media

W. Klinbun [a], K. Vafai [b,*], P. Rattanadecho [c]

[a] Rattanakosin College for Sustainable Energy and Environment (RCSEE), Rajamangala University of Technology Rattanakosin, 96 moo 3, Puthamonthon Sai 5, Salaya, Puthamonthon, Nakhon Pathom 73170, Thailand
[b] Department of Mechanical Engineering, University of California, A363 Bourns Hall, Riverside, CA, 2507-0425, USA
[c] Department of Mechanical Engineering, Thammasat University (Rangsit Campus), 99 moo 18, Klong Luang, Pathum Thani 12120, Thailand

ARTICLE INFO

Article history:
Received 30 May 2011
Received in revised form 30 August 2011
Accepted 30 August 2011
Available online 6 October 2011

Keywords:
Forced convection
Electromagnetic field
Thermal dispersion
Local thermal non equilibrium (LTNE)
Porous medium

ABSTRACT

The effect of an imposed electromagnetic field on forced convection in porous media is analyzed in this work. The transient Maxwell's equations are solved to simulate the electromagnetic field inside the waveguide and within a porous medium. The Brinkman–Forchheimer extended Darcy (generalized model) equations are used to represent the flow fluid inside a porous medium. The local thermal non-equilibrium (LTNE) is taken into account by solving the two-energy equation model for fluid and solid phases. Computational domain is represented for a range of Darcy number from 10^{-5} to 10^{-7} and dimensionless electromagnetic wave power P^* from 0 to 1600, and dimensionless electromagnetic wave frequency f^* from 0 to 8. The effect of variations of the pertinent electromagnetic field parameters in affecting the flow and thermal fields and the Nusselt number are analyzed. This investigation provides the essential aspects for a fundamental understanding of forced convection in porous media while experiencing an applied electromagnetic field such as applications in the material-processing field.

1. Introduction

Various engineering applications are based on forced convection through a porous medium. For example, cooling of nuclear waste container, catalytic, heat transfer enhancement devices, chemical reactors, solar power collectors, drying processes, combustion and ceramic processing to name a few. As such transport through porous media has been of interest for many decades. Two different models are used for analyzing heat transfer in a porous medium; local thermal equilibrium (LTE) and local thermal non-equilibrium (LTNE). Most of the prior works are based on invoking the local thermal equilibrium assumption; i.e., the solid phase temperature is equal to fluid phase temperature everywhere in the porous medium. However, this assumption is not valid for a number of physical situations such as when the fluid flows at a high speed through the porous medium. In recent years, the local thermal non-equilibrium model in a porous medium has received more attention as demonstrated by the works of Vafai and Sozen [1–3] and further pursued by Quintard and Whitaker [4], Quintard [5], Amiri and Vafai [6], Kuznetsov [7] and Nakayama et al. [8] and many others. Jiang and Ren [9] and Jiang et al. [10] used local thermal non-equilibrium model to investigate forced convective heat transfer in a channel filled with a porous medium. They studied the effect of thermal dispersion, variable properties, and particle diameter, particle thermal conductivity and appropriate boundary conditions. The numerical results were in agreement with their experimental data.

Another important parameter affecting the transport phenomena in a porous medium is thermal dispersion. Dispersion needs to be considered if the filtration velocity is large enough for the Forchheimer term to be significant. Amiri and Vafai [6] illustrated the important role of transverse thermal dispersion on forced convection heat transfer in porous media. In addition, according to Kuo and Tien [11], Hsu and Cheng [12], Hunt and Tien [13], Sozen and Vafai [14], Nield [15], and Kuznetsov et al. [16], longitudinal thermal dispersion effects can usually be neglected without causing any significant errors in heat transfer results. However, Kuwahara and Nakayama [17] have suggested that the longitudinal thermal dispersion should also be taken into account. As such for this work, both longitudinal and transverse thermal dispersions will be considered. Electromagnetic wave is an important heat source that is applied in many industrial and household applications since electromagnetic wave can penetrate the surface and is converted into thermal energy very rapidly within the material. There have been a number investigations of natural convection under electromagnetic field, such as Bian et al. [18], Ni et al. [19], Ratanadecho et al. [20], Rattanadecho et al. [21,22], Shigemitsu et al. [23], Wang et al. [24], Dinčov et al. [25], Basak and Meenakshi [26], Cha-um et al. [27] and others. However, the effect of electromagnetic field on forced convection in a porous medium particularly under non-thermal equilibrium is not well understood. There are various effects related to the effects of

* Corresponding author. Tel.: +1 951 827 3125; fax: +1 951 827 2899.
E-mail address: vafai@engr.ucr.edu (K. Vafai).

0017-9310/$ - see front matter © 2011 Elsevier Ltd. All rights reserved.
doi:10.1016/j.ijheatmasstransfer.2011.09.022

Nomenclature

a_1, a_2	porosity variation parameters, Eq. (24)
a_{sf}	specific surface area of the packed bed (m^{-1})
C_p	specific heat capacity ($J\,kg^{-1}\,K^{-1}$)
d_p	particle diameter (m)
Da	Darcy number, K_∞/H^2
E	electric field intensity ($V\,m^{-1}$)
F	the geometric function defined in Eq. (18)
f	frequency of incident wave (Hz)
h_{sf}	fluid-to-solid heat transfer coefficient ($W\,m^{-2}\,K^{-1}$)
H	magnetic field intensity ($A\,m^{-1}$)
H	height of the packed bed (m)
J	unit vector oriented along the pore velocity vector, $V_p/\lvert V_p\rvert$
k	thermal conductivity ($W\,m^{-1}\,K^{-1}$)
K	permeability (m^2)
L	length of the packed bed (m)
LTE	local thermal equilibrium
Nu	Nusselt number
Pr	Prandtl number, $\mu C_{pf}/k_f$
P	power (W)
p	pressure (Pa)
Q	local electromagnetic heat generation term ($W\,m^{-3}$)
Re_p	particle Reynolds number, $\rho_f u_e d_p/\mu$
t	time (s)
T	temperature (K)
tan δ	dielectric loss coefficient (–)
u	velocity component in the x-direction (ms^{-1})
V	velocity vector (ms^{-1})
x, y	Cartesian coordinates (m)
Z_H	wave impedance (), $\frac{\lambda_g}{\lambda}\sqrt{\frac{\phi}{\gamma}}$

Greek letters

α	thermal diffusivity ($m^2\,s^{-1}$)
ε	porosity (–)
η	dimensionless vertical scale defined in Eq. (35)
θ	dimensionless fluid phase temperature
Θ	dimensionless solid phase temperature
γ	permittivity ($F\,m^{-1}$)
φ	magnetic permeability ($H\,m^{-1}$)
λ	wavelength (m)
μ	dynamic viscosity ($kg\,m^{-1}\,s^{-1}$)
ρ	density ($kg\,m^{-3}$)
σ	electric conductivity ($S\,m^{-1}$)
ξ	dimensionless length scale defined in Eq. (37)

Subscripts

e	inlet
f	fluid
eff	effective property
m	mean
s	solid
w	wall
x, y, z	x, y, z-component
∞	asymptotic or free stream

Superscripts

c	cutoff
f	fluid
s	solid
*	dimensionless quantity

Symbols

$\langle\rangle$	'local volume average' of a quantity

an imposed electromagnetic field on non-thermal equilibrium and dispersion in a porous medium that are not well understood and several pertinent issues remain unresolved.

The objective of this study is to analyze and demonstrate the effect of electromagnetic field on forced convection in a fluid-saturated porous medium. The effects of the dimensionless electromagnetic wave power (P^*), and dimensionless electromagnetic wave frequency (f^*) on the dimensionless temperature field and Nusselt number distribution are discussed. The porous medium is considered to be a packed bed of spherical particles saturated with a fluid.

2. Analysis

Forced convection of an incompressible fluid flow through a packed bed of spherical particles subjected to an electromagnetic field as shown in Fig. 1 is considered. The configuration consists of a porous medium that fills inside a rectangular waveguide. Walls of the guide are assumed to be made of metal which approximates a perfect electrical conductor. The monochromic wave in fundamental mode (TE_{10}) is applied in the x-direction. The domain in which the electromagnetic field is analyzed includes the entire region enclosed by the walls of the guide. For temperature and flow fields the computational domain is limited to the region enclosed by the container. The horizontal walls of container are kept at a constant temperature.

2.1. Analysis of the electromagnetic field

Maxwell's equations for TE_{10} mode are solved to obtain the electromagnetic field inside a rectangular waveguide and the enclosed porous medium.

Maxwell's equations for TE_{10} mode [20]:

$$E_y = E_x = H_z = 0, \tag{1}$$

$$\frac{\partial E_z}{\partial t} = \frac{1}{\gamma}\left(\frac{\partial H_y}{\partial x} - \frac{\partial H_x}{\partial y} - \sigma E_z\right), \tag{2}$$

$$\frac{\partial H_x}{\partial t} = -\frac{1}{\phi}\left(\frac{\partial E_z}{\partial y}\right), \tag{3}$$

$$\frac{\partial H_y}{\partial t} = \frac{1}{\phi}\left(\frac{\partial E_z}{\partial x}\right), \tag{4}$$

where E and H are the electric and magnetic fields, $\gamma = \gamma_0\gamma_r = \gamma_0(\gamma_r' - j\gamma_r'')$ is electric permittivity, $\phi = \phi_0\phi_r$ is magnetic permeability, and σ is electric conductivity.

Boundary and initial conditions:

(1) At the walls of the waveguide and cavity, a perfect conducting condition is considered. Therefore, normal components of the magnetic field and tangential components of the electric field vanish at these walls [20]:

$$H_n = 0, \quad E_t = 0. \tag{5}$$

(2) At the absorbing plane, Mur's first order absorbing condition is utilized [20]:

$$\frac{\partial E_z}{\partial t} = \pm c\frac{\partial E_z}{\partial x}, \tag{6}$$

where ± represents forward and backward directions and c denotes the phase velocity of the propagation wave.

(3) At the incident plane, the input microwave source is simulated by [20]:

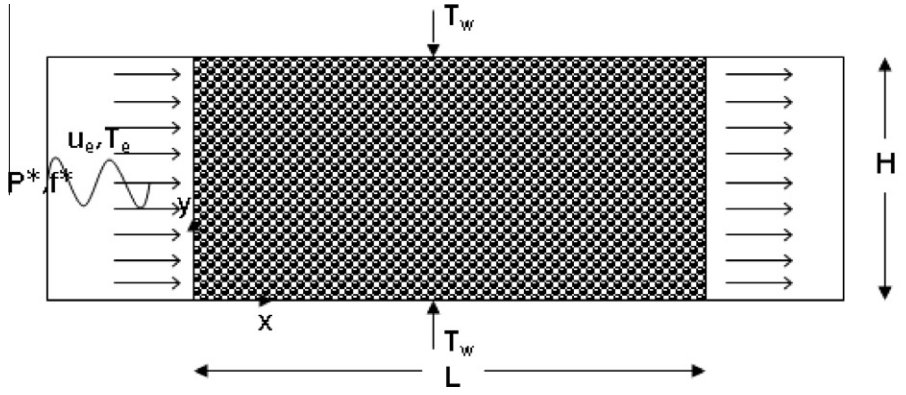

Fig. 1. Schematic diagram of the problem under consideration and the corresponding coordinate system.

Table 1
Thermal and dielectric properties used in the computations [6,20,26].

Material property	Air	Water	Lead	Alumina	Soda lime
Density, ρ(kg m^{-3})	1.1	989	7660	3750	2225
Specific heat, C_p(J kg^{-1} K^{-1})	1008	4180	448	1046	835
Thermal conductivity, k(Wm^{-1} K^{-1})	0.028	0.640	82	26	1.4
Viscosity, μ(kg m^{-1} s^{-1}) $\times 10^5$	1.9	57.7	–	–	–
Dielectric constant, γ_r	1.0	$88.15 - 0.414T + (0.131 \times 10^{-2})T^2 - (0.046 \times 10^{-4})T^3$	6.9	10.8	7.5
Loss tangent, tan δ	0.0	$0.323 - (9.499 \times 10^{-3})T + (1.27 \times 10^{-4})T^2 - (6.13 \times 10^{-7})T^3$	0.0139	0.0145	0.0125

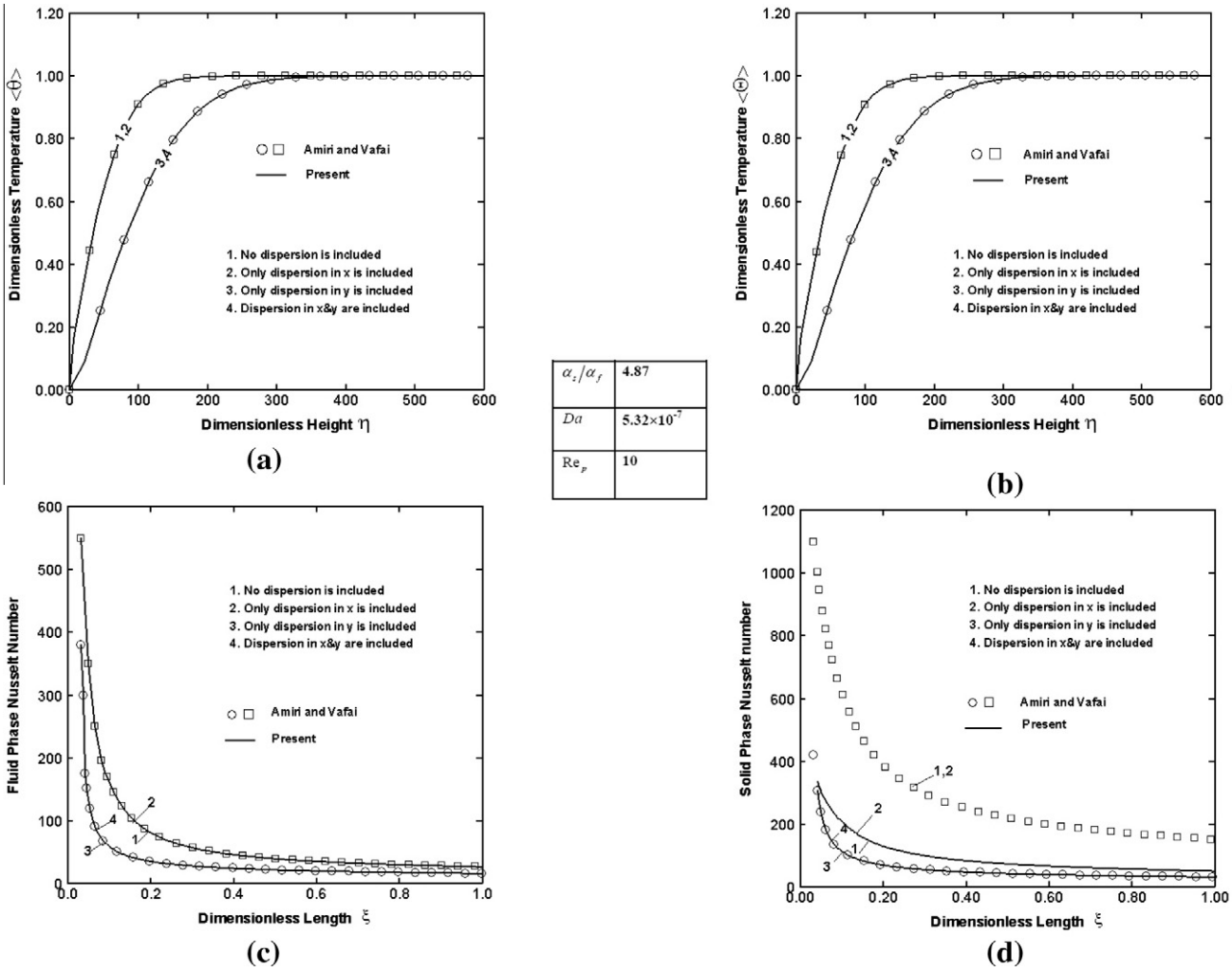

Fig. 2. Comparison of dimensionless temperature and the Nusselt number distributions for the present work versus the results of Amiri and Vafai [6] for $\alpha_s/\alpha_f = 4.87$, $Da = 5.32 \times 10^{-7}$ and $Re_p = 10$.

$$E_{z,Inc.} = E_{zin} \sin\left(\frac{\pi y}{a}\right) \sin(2\pi f t), \tag{7}$$

$$H_{y,Inc.} = \frac{E_{zin}}{Z_H} \sin\left(\frac{\pi y}{a}\right) \sin(2\pi f t), \tag{8}$$

where f is the frequency of microwave, a is the width of the incidence plane, Z_H is the wave impedance, and E_{zin} is the input value of the electric field intensity. By applying the Poynting theorem, the input value of the electric field intensity is evaluated by the microwave input power as [20]:

$$E_{zin} = \sqrt{\frac{4 Z_H P_{in}}{A}}, \tag{9}$$

where P_{in} is the microwave power input and A is the area of the incident plane.

(4) At the interface between different materials, for example air and the porous medium, the continuity condition is invoked as:

$$E_t = E'_t, \quad H_t = H'_t, \tag{10}$$

$$D_n = D'_n, \quad B_n = B'_n. \tag{11}$$

(5) At $t = 0$ all components of E, H are zero.

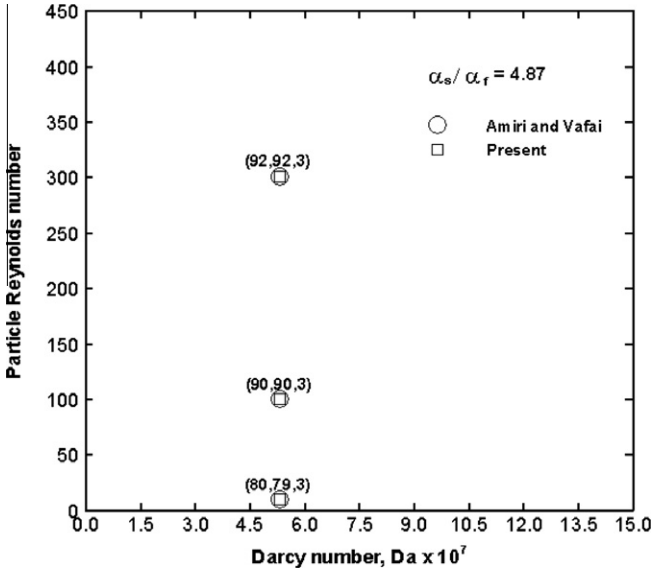

Fig. 3. Comparison of percent error on the average fluid Nusselt number for the present work versus the results of Amiri and Vafai [6] for $\alpha_s/\alpha_f = 4.87$, $Da = 5.32 \times 10^{-7}$ and $Re_p = 10$.

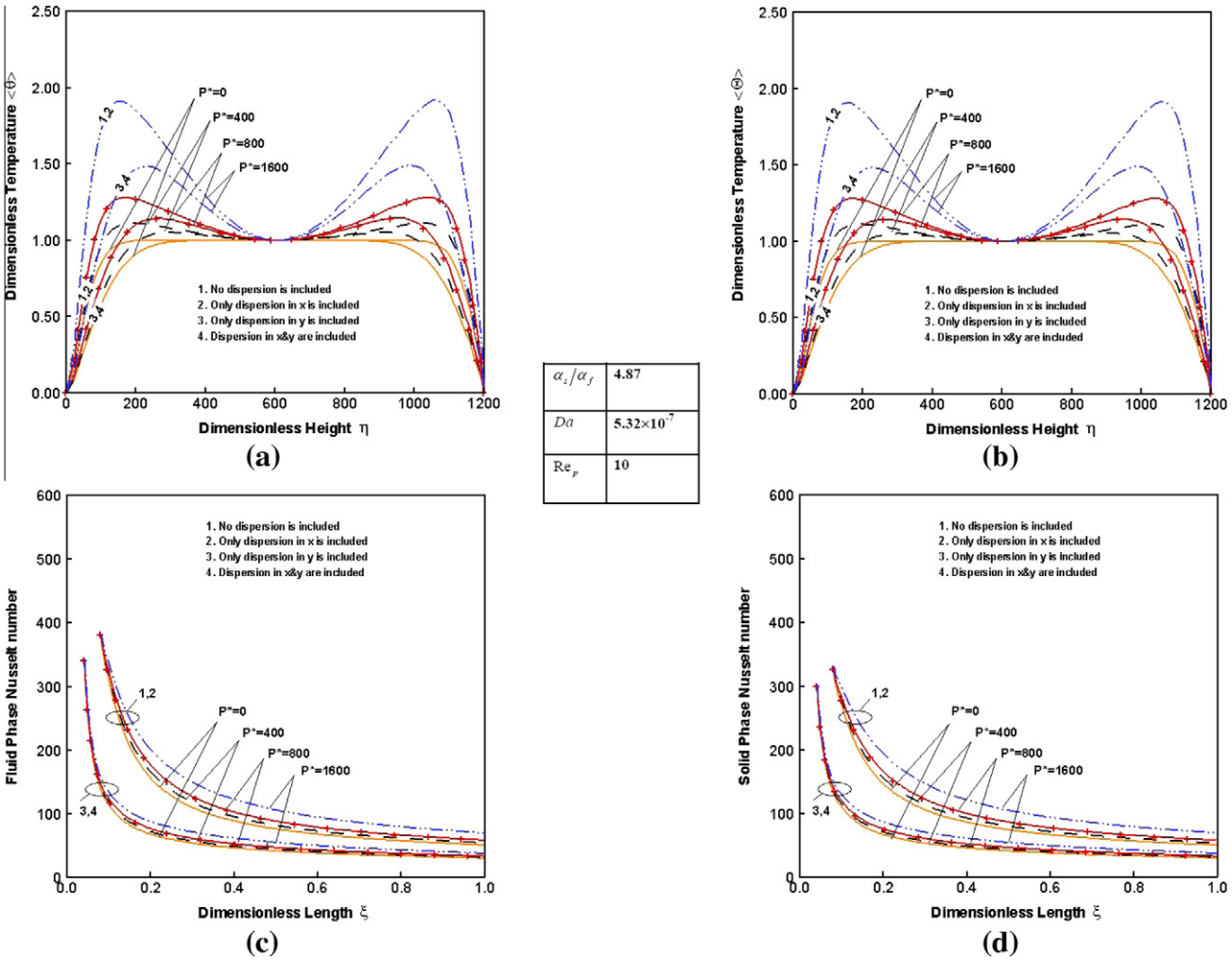

Fig. 4. Effects of the variations in the electromagnetic field power on the temperature field and the Nusselt number distribution for $\alpha_s/\alpha_f = 4.87$, $Da = 5.32 \times 10^{-7}$, $Re_p = 10$ and $f^* = 4.0$.

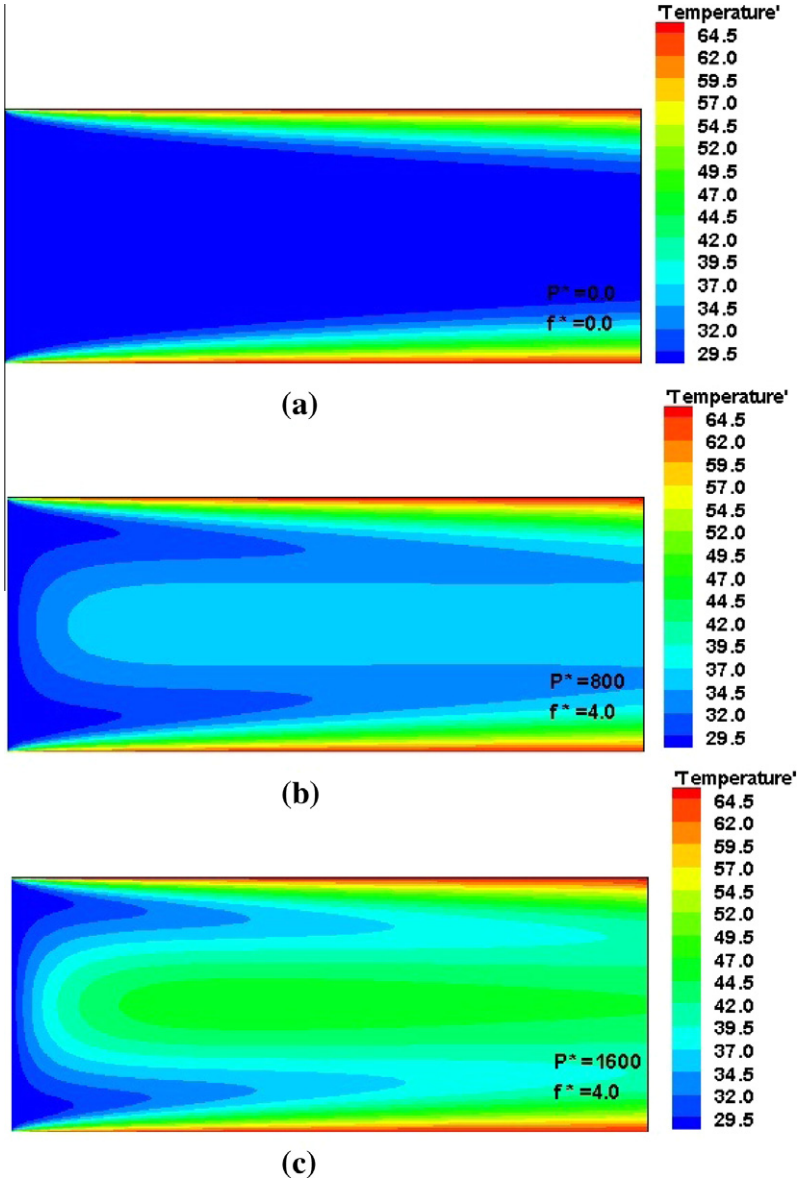

Fig. 5. Fluid phase temperature contour in the x–y plane at $\alpha_s/\alpha_f = 4.87$, $Da = 5.32 \times 10^{-7}$, $Re_p = 10$ and $f^* = 4.0$ incorporating the variable porosity as well as the axial and lateral thermal dispersions.

2.2. Analysis of flow and heat transfer within a porous medium

The schematic configuration of the problem is shown in Fig. 1, where H and L denote the height and length of the packed bed, respectively. The porous medium is considered homogenous, isotropic and is saturated with a fluid. Furthermore, the solid particles are considered to be spherical, uniform shape, and incompressible. The steady state volume-averaged governing equations are [6]

Continuity equation:

$$\nabla \cdot \langle V \rangle = 0. \tag{12}$$

Momentum equation [6]:

$$\frac{\rho_f}{\varepsilon}\langle (V \cdot \nabla)V \rangle = -\frac{\mu}{K}\langle V \rangle - \frac{\rho_f F \varepsilon}{\sqrt{K}}[\langle V \rangle \cdot \langle V \rangle]J + \frac{\mu}{\varepsilon}\nabla^2 \langle V \rangle - \nabla \langle p \rangle^f. \tag{13}$$

Fluid phase energy equations [6]:

$$\varepsilon \langle \rho_f \rangle^f C_{pf} \frac{\partial \langle T_f \rangle^f}{\partial t} + \langle \rho_f \rangle^f C_{pf} \langle V \rangle \cdot \nabla \langle T_f \rangle^f = \nabla \cdot \left\{ k_{feff} \cdot \nabla \langle T_f \rangle^f \right\} + h_{sf} a_{sf} \left(\langle T_s \rangle^s - \langle T_f \rangle^f \right) + \varepsilon Q_f. \tag{14}$$

Solid phase energy equations [6]:

$$(1-\varepsilon)\rho_s C_{ps} \frac{\partial \langle T_s \rangle^s}{\partial t} = \nabla \cdot \left\{ k_{seff} \cdot \nabla \langle T_s \rangle^s \right\} - h_{sf} a_{sf} \left(\langle T_s \rangle^s - \langle T_f \rangle^f \right) + (1-\varepsilon) Q_s \tag{15}$$

where Q is the local electromagnetic heat generation term, which is a function of the electric field and defined as [20]:

$$Q = 2\pi f \gamma_0 \gamma_r' (\tan \delta) E_z^2, \tag{16}$$

where γ_r' is the relative dielectric constant. The permeability of the packed bed and the geometric function are [6]:

$$K = \frac{\varepsilon^3 d_p^2}{150(1-\varepsilon)^2}, \tag{17}$$

$$F = \frac{1.75}{\sqrt{150\varepsilon^3}}. \tag{18}$$

The specific surface area of the packed bed can be represented as [6]:

$$a_{sf} = \frac{6(1-\varepsilon)}{d_p}. \tag{19}$$

The formulation of the fluid-to-solid heat transfer coefficient in this study is expressed as [6]:

$$h_{sf} = k_f \left[2 + 1.1\mathrm{Pr}^{1/3} \left(\frac{\rho_f u d_p}{\mu_f} \right)^{0.6} \right] \Big/ d_p, \tag{20}$$

when the thermal dispersion effects are present, axial and lateral effective conductivities of fluid phase can be expressed, respectively, as [6]:

$$(k_{feff})_x = \left[\varepsilon + 0.5\mathrm{Pr} \left(\frac{\rho_f u d_p}{\mu} \right) \right] k_f, \tag{21}$$

$$(k_{feff})_y = \left[\varepsilon + 0.1\mathrm{Pr} \left(\frac{\rho_f u d_p}{\mu} \right) \right] k_f, \tag{22}$$

$$k_{seff} = (1-\varepsilon) k_s. \tag{23}$$

In addition, the variation of porosity near the impermeable boundaries can be expressed as [6]:

$$\varepsilon = \varepsilon_\infty \left[1 + a_1 \exp\left(\frac{-a_2 y}{d_p} \right) \right], \tag{24}$$

where ε_∞ is the free stream porosity while a_1, a_2 are empirical constants.

The Nusselt number for both phases can be expressed as [6]:

$$Nu_f = -\frac{2\mathrm{H}}{T_w - T_{mf}} \left(\frac{\partial \langle T_f \rangle^f}{\partial y} \right)_{y=0}, \tag{25}$$

$$Nu_s = -\frac{2\mathrm{H}}{T_w - T_{ms}} \left(\frac{\partial \langle T_s \rangle^s}{\partial y} \right)_{y=0}. \tag{26}$$

where T_{mf} and T_{ms} are the mixed mean temperatures of the fluid and solid phases, respectively which can be expressed as [6]:

$$T_{mf} = \frac{1}{U_m H} \int_0^H u T_f dy, \tag{27}$$

$$T_{ms} = \frac{1}{H} \int_0^H T_s dy, \tag{28}$$

where

$$U_m = \frac{1}{H} \int_0^H u dy. \tag{29}$$

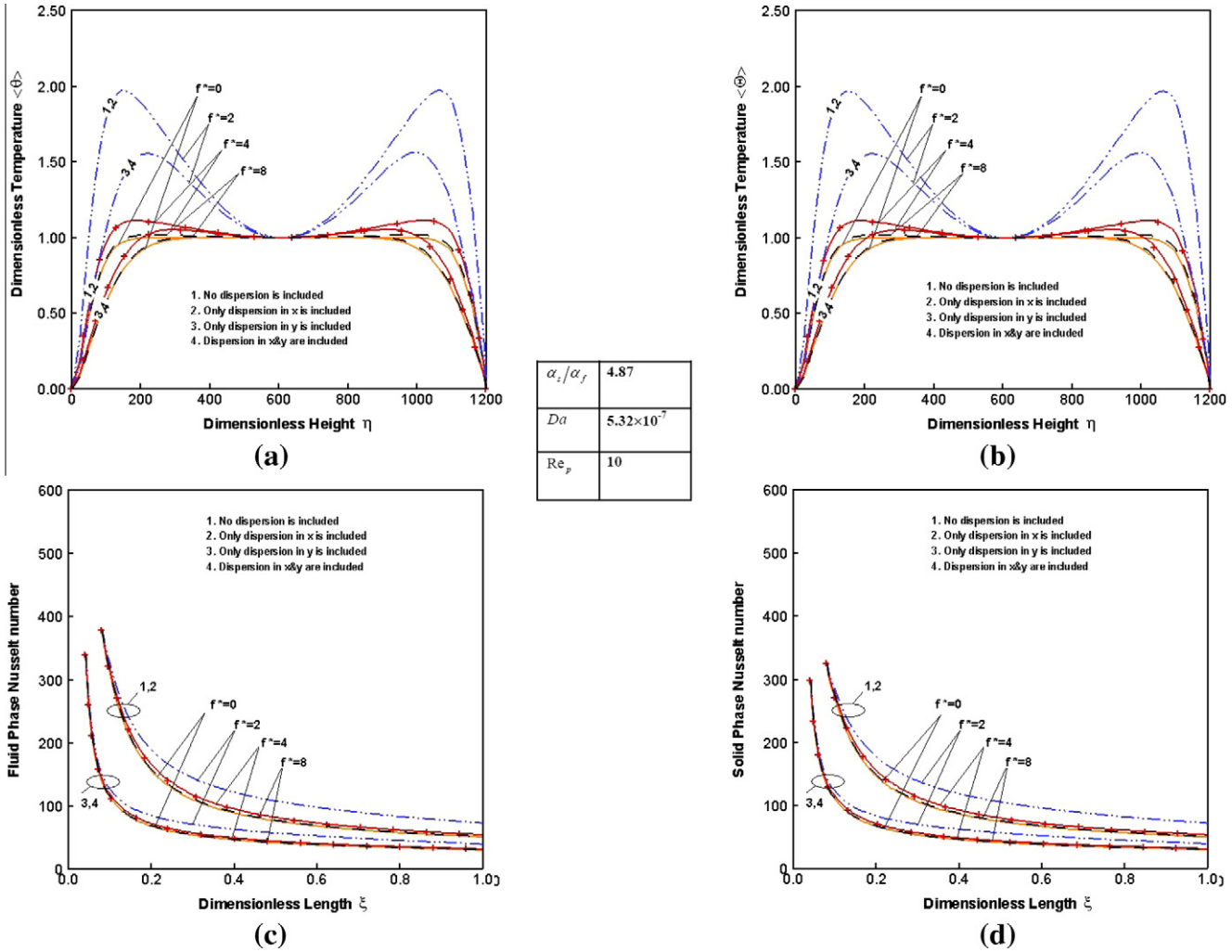

α_s/α_f	4.87
Da	5.32×10^{-7}
Re_p	10

Fig. 6. Effect of the electromagnetic field frequency on the temperature field and Nusselt number distribution for $\alpha_s/\alpha_f = 4.87$, $Da = 5.32 \times 10^{-7}$, $Re_p = 10$ and $P^* = 400$.

Boundary and initial conditions:

From Fig. 1, no slip boundary conditions are applied at all the solid walls which are kept at a constant temperature. Thus, the boundary conditions are as follows:

$$u(x,y) = 0 \quad \text{at } y = 0,\ H, \tag{30}$$

$$T_f(x,y) = T_s(x,y) = T_w \quad \text{at } y = 0,\ H, \tag{31}$$

$$T_f(x,y) = T_s(x,y) = T_e \quad \text{at } x = 0, \tag{32}$$

The inlet and wall temperature are taken as:

$T_e = 300\,K, \quad T_w = 340\,K.$

A particle diameter of 5.0 mm is used in the computations. The Dielectric and thermal properties are listed in Table 1 [6,20,26].

3. Numerical simulations

Maxwell's equations (Eqs. (2)–(4)), are solved using the finite difference method. The electric (E) and magnetic (H) field components are discretized using a central differencing scheme (second-order) in both space and time domains. The equations are solved using the leap-frog methodology; the electric field is solved at a given time step, the magnetic field is solved at the next time step, and the process is repeated sequentially. The fluid flow and heat transport within a porous medium are expressed through Eqs. (12)–(15). These equations are coupled to Maxwell's equations through Eq. (16). Eqs. (12)–(15) are solved numerically using a finite control volume approach along with the SIMPLE algorithm [28]. The proposed discretization conserves the fluxes and avoids generation of a parasitic source. The basic strategy for the finite control volume discretization method is to divide the computational domain into a number of control volumes and then integrate the conservation equations over this control volume within an interval of time $[t, t + \Delta t]$. At the boundaries of the computational domain, integrating over half the control volume and taking into account the boundary conditions discretizes the conservation equations and at the corners a quarter of the control volume is utilized. The fully implicit time discretization finite difference scheme is used to arrive at the solution in time. To insure

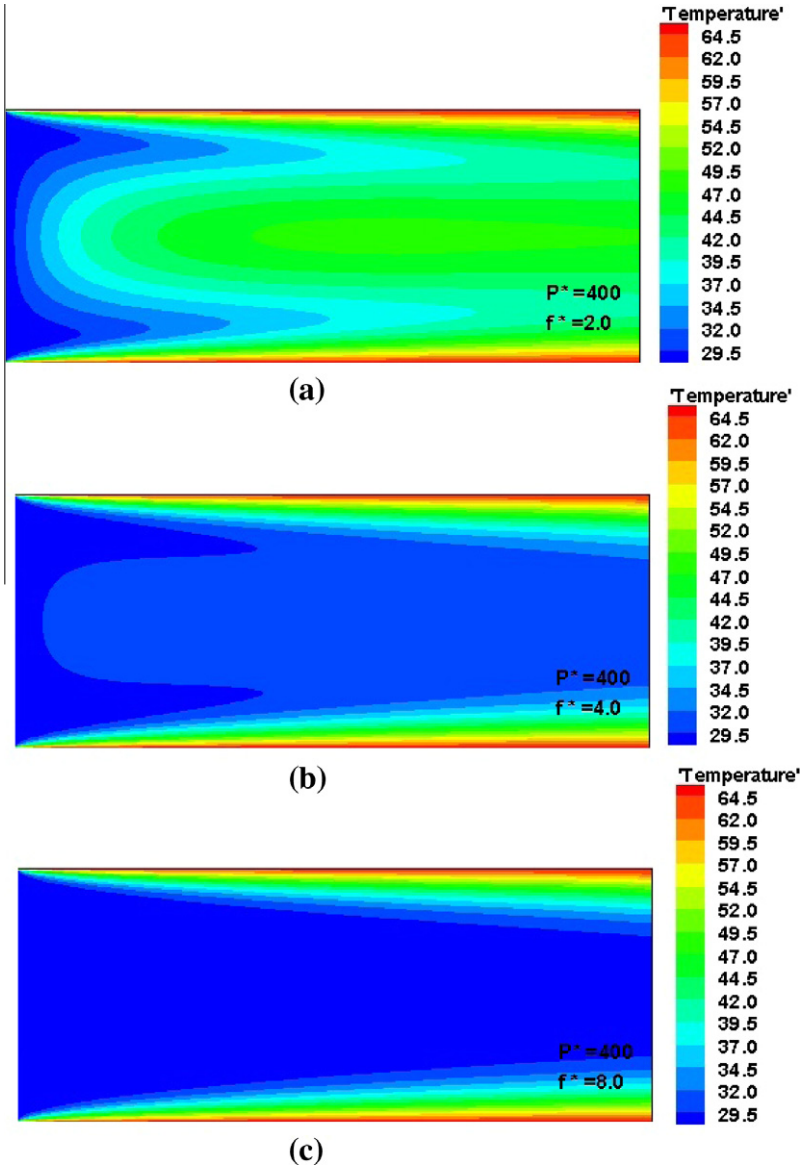

Fig. 7. Fluid phase temperature contour in the x–y plane at $\alpha_s/\alpha_f = 4.87$, $Da = 5.32 \times 10^{-7}$, $Re_p = 10$ and $P^* = 400$ incorporating the variable porosity as well as the axial and lateral thermal dispersions.

stability of the time-stepping algorithm Δt is chosen to satisfy the courant stability condition [20]:

$$\Delta t \leqslant \frac{\sqrt{(\Delta x)^2 + (\Delta y)^2}}{c}, \tag{33}$$

and the spatial resolution of each cell satisfies:

$$\Delta x,\ \Delta y \leqslant \frac{\lambda_g}{10\sqrt{\gamma_r}}, \tag{34}$$

where λ_g is the wavelength of microwave in the rectangular waveguide and γ_r is the relative electric permittivity.

The following set of simulation parameters are used to satisfy conditions given by Eqs. (33) and (34):

(1) *Grid size:* $\Delta x = 1.0$ mm and $\Delta y = 1.0$ mm.
(2) *Time steps:* $\Delta t = 2 \times 10^{-12}$ s and $\Delta t = 0.01$ s are used corresponding to electromagnetic field and temperature field calculations, respectively.
(3) Relative error in the iteration procedures is ensured to be less than 10^{-6}.

4. Results and discussion

4.1. Validation

The computational results are validated with the numerical results by Amiri and Vafai [6]. The following parameters are used to generate the results: $d_p = 5$ mm, $\varepsilon_\infty = 0.37$, $a_1 = 1.7$, $a_2 = 6$, $\alpha_s/\alpha_f = 4.87$, $Da = 5.32 \times 10^{-7}$ and $Re_p = 10$. The comparison of dimensionless temperature fields, Nusselt number distributions and percent error on the average Nusselt numbers are displayed in Figs. 2 and 3. Fig. 3 illustrates the comparison of the percent error on the average fluid Nusselt number. Overall, our results (other than the apparent misplaced curve of Vafai and Amiri [6] for cases 1 & 2 in Fig. 2(d)) are in excellent agreement with those by Amiri and Vafai [6].

The results are presented in a non-dimensional form, such as dimensionless fluid and solid phase temperature. These dimensionless groups are defined as: $\theta = (T_w - T_f)/(T_w - T_{mf})$, $\Theta = (T_w - T_s)/(T_w - T_{ms})$. The temperature field and Nusselt number are plotted against a dimensionless vertical scale, η, and a dimensionless length, ξ respectively defined as [6]:

$$\eta = \frac{y\gamma_\infty}{\xi^{1/2}}, \tag{35}$$

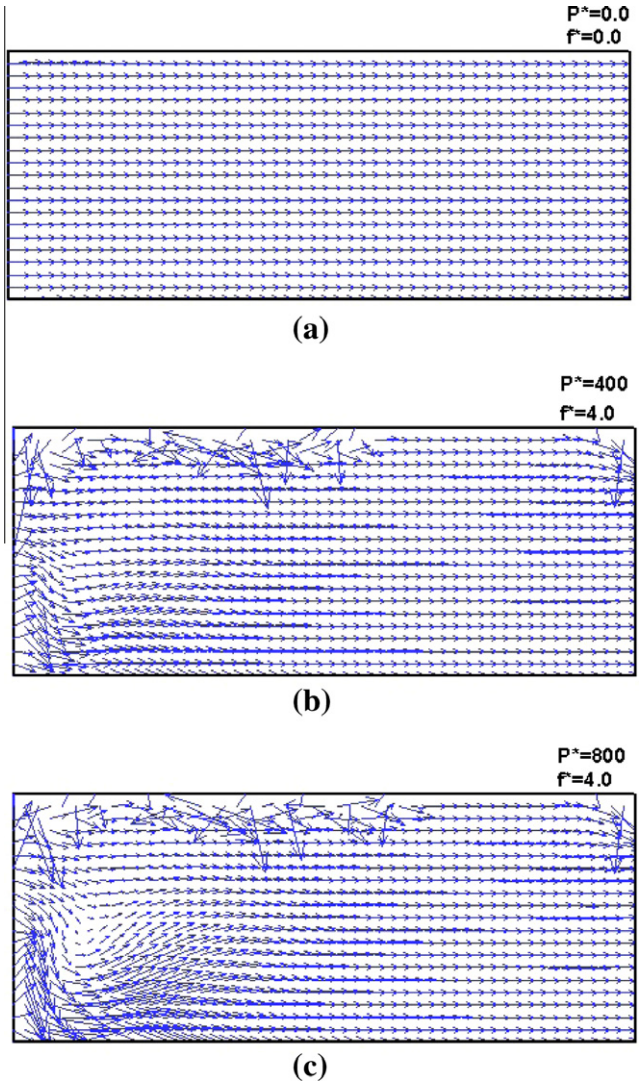

Fig. 8. Flow field in the x–y plane for $\alpha_s/\alpha_f = 4.87$, $Da = 5.32 \times 10^{-7}$, $Re_p = 0.1$ and $f^* = 4.0$ incorporating the variable porosity as well as the axial and lateral thermal dispersions.

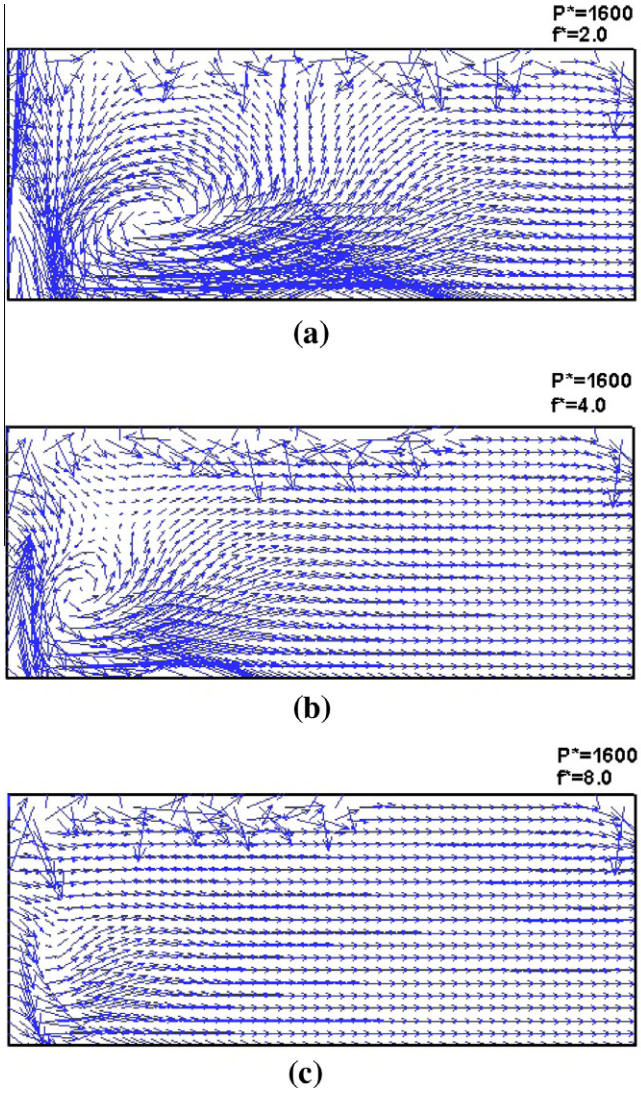

Fig. 9. Flow field in the x–y plane for $\alpha_s/\alpha_f = 4.87$, $Da = 5.32 \times 10^{-7}$, $Re_p = 0.1$ and $P^* = 1600$ incorporating the variable porosity as well as the axial and lateral thermal dispersions.

where γ_∞ is the free stream shape parameter and ξ is the dimensionless length scale expressed as [6]:

$$\gamma_\infty = \sqrt{\frac{\varepsilon_\infty}{K_\infty}}, \tag{36}$$

$$\xi = \frac{x}{L}. \tag{37}$$

The temperature profile and velocity field are presented at the middle of the porous medium or $\xi = 0.5$.

The dimensionless electromagnetic power and electromagnetic frequency are defined as:

$$P^* = \frac{P}{k_f H(T_w - T_e)}, \tag{38}$$

$$f^* = \frac{f}{f_{c10}}, \tag{39}$$

where f_{c10} is the cut off frequency (lowest propagation frequency) of the microwave in TE_{10} mode.

4.2. Thermal dispersion effects

The effects of electromagnetic field on thermal dispersion are presented in Figs. 4–7. The physical data utilized in these figures are: $\alpha_s/\alpha_f = 4.87$, $Da = 5.32 \times 10^{-7}$ and $Re_p = 10$. Fig. 4 shows the effects of variations in the electromagnetic field power. The non-dimensional power varies from 0 to 1600 at $f^* = 4.0$. The dimensionless temperature fields are shown in Fig. 4(a) and (b) while Fig. 4(c) and (d) demonstrate the Nusselt number distributions. As expected, both of the temperature and the Nusselt number values increase with an increase in the electromagnetic power. This is because an increase in the electromagnetic power results in a higher heat generation rate inside the packed bed. It can be observed that the temperature and Nusselt number values are higher when thermal dispersion is excluded (case 1) as compared to when it is included (case 4). The results reveal that the longitudinal dispersion can be neglected as it does not affect the results. Fig. 5 shows the temperature contours in the x–y plane while incorporating the variable porosity and dispersion effects. As can be seen in Fig. 5, besides the walls, higher temperatures occur in the middle of the packed bed because the electric field density in the TE_{10} mode is high around the center region of the waveguide.

Figs. 6 and 7 illustrate the effect of variations in the electromagnetic field frequency. The frequency is varied from 0 to 8 at $P^* = 400$. Fig. 6(a) and (b) show the dimensionless temperature profile whereas the Nusselt number distributions are depicted in Fig. 6(c) and (d), respectively. Fig. 7 displays the effect of variations in the electromagnetic frequency on the fluid phase temperature contours. The temperature profiles (Fig. 6) qualitatively follows the temperature contour plots (Fig. 7). The results show that the highest temperature values do not correspond to the highest electromagnetic frequencies. The highest temperature values, for the cases considered here, correspond to $f^* = 2.0$, while $f^* = 8.0$ produces the lowest values of the temperature and Nusselt numbers. Our results have established the existence of an optimum value for the frequency in terms of attaining the maximum temperature within the porous medium. This is because a high frequency electromagnetic wave has a short wavelength and a smaller penetration depth than a low frequency wave. Thus most electromagnetic waves are absorbed at the entrance region of the medium.

Figs. 8 and 9 show the effect of variations in the electromagnetic power and frequency on the flow field. The electromagnetic power variations from 0 to 1600 at $f^* = 2.0$ and frequency variations from 0 to 8 at $P^* = 1600$ are considered. The results are shown for: $\alpha_s/\alpha_f = 4.87$, $Da = 5.32 \times 10^{-7}$ and $Re_p = 0.1$. Flow fields within the sample at different powers are displayed in Figs. 8(b), (c) and 9(b). As can be clearly seen the fluid movement is further augmented as the power increases. The fluid circulation starts from a corner near the inlet surface where the incident wave propagates through it. Fig. 9(a)–(c) depict the flow patterns at non-dimensionalized electromagnetic frequencies of 2, 4 and 8, respectively. The fields are somewhat similar. However, the magnitudes of velocities are significantly altered. Based on the earlier assessment from Fig. 6, the largest flow augmentation is expected to occur at $f^* = 2.0$. Fig. 9 confirms this expectation.

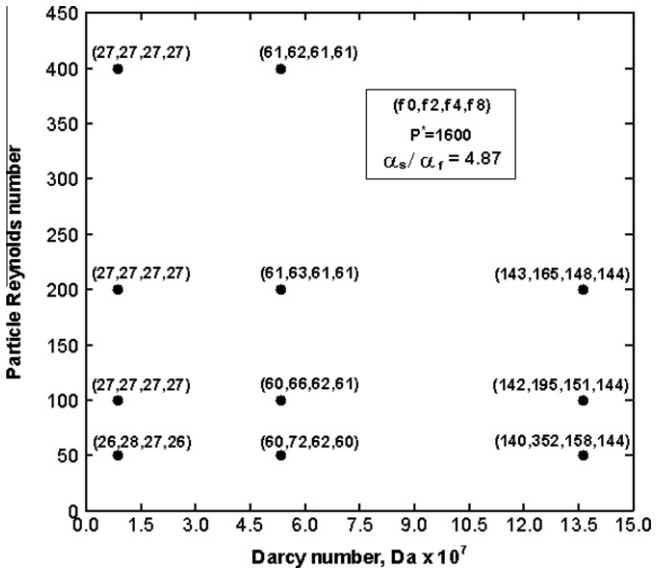

Fig. 10. Effect of the frequency variations on the average fluid Nusselt number while accounting for both axial and transverse thermal dispersion effects ($\alpha_s/\alpha_f = 4.87$, $P^* = 1600$).

Fig. 10 shows the effect of frequency variations on the average fluid Nusselt numbers while incorporating the axial and transverse thermal dispersion effects. The Nusselt number values are given within the parenthesis in Fig. 10. The non-dimensionalized electromagnetic frequencies are varied from 0 to 8 at $P^* = 1600$. It is found that the Darcy number is the primary parameter that affects the magnitude of the Nusselt numbers. It is also shown that the $f^* = 2.0$ has a more profound effect on the heat transfer process.

4.3. Local thermal equilibrium (LTE) assumption

In order to examine the local thermal equilibrium assumption, the temperature distributions for the fluid and solid are considered at all point. We define a percent variation in the temperature values compared to those obtained based on the LTE assumption [6]:

$$\%LTE = \left|\theta_{(i,j)} - \Theta_{(i,j)}\right| \times 100.$$

The extent of variations in the temperature values is used to classify the appropriateness of the LTE assumption. The qualitative ratings for LTE assumption [6] are expressed as: less than 1% as very good, 1–5% as good, 5–10% as fair, 10–15% as poor and more than 15% as very poor. Fig. 11 demonstrates the qualitative assessment with respect to the LTE assumption for a substantial range of variations in the thermophysical properties. As such the results are presented for α_s/α_f equal to 4.87 and 42.82, respectively while incorporating the porosity variation and thermal dispersion effects. The case without any electromagnetic effect is presented in Fig. 11(a) and (d) [6] as a benchmark to assess the electromagnetic field effect on LTE. Fig. 11(b)–(f) show the effects of the electromagnetic power and frequency on the validity of the LTE assumption. It can be clearly seen that in addition to the Darcy and the particle Reynolds numbers, electromagnetic power has a substantial effect on the validity of the LTE assumption.

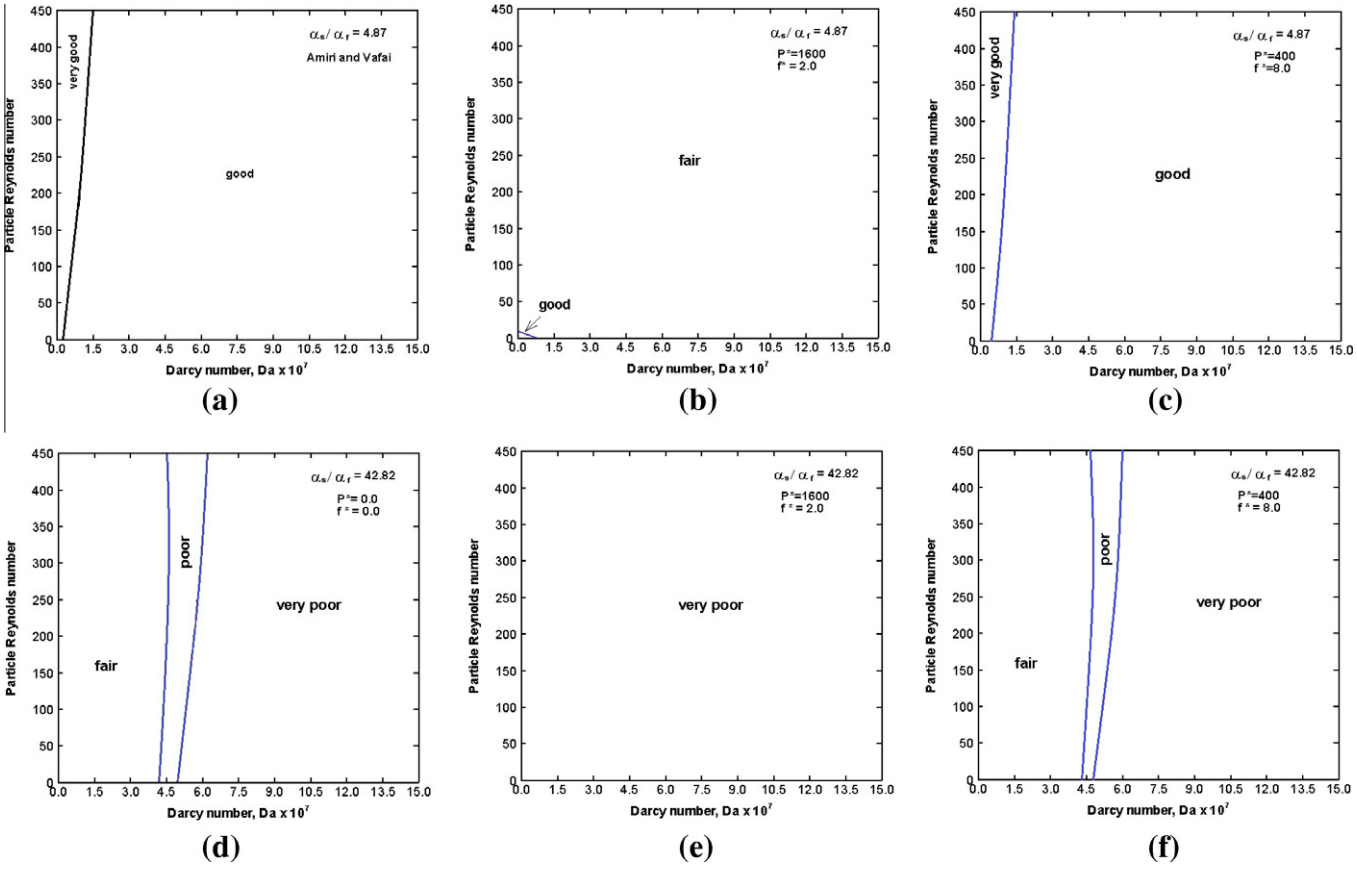

Fig. 11. Qualitative assessment for LTE for the cases with α_s/α_f equal to 4.87 and 42.82 incorporating the variable porosity as well as the axial and lateral thermal dispersions.

As can be seen the local thermal equilibrium assumption deteriorates as the Darcy number (Da) or the solid-to-fluid thermal diffusivity ratio or the electromagnetic power (P^*) increase.

5. Conclusions

The effect of an electromagnetic field on transport through a porous medium is analyzed in this work. To this end, the transient Maxwell's equations are utilized to describe the electromagnetic field distribution inside the waveguide and the porous medium while the flow field is simulated using the Brinkman–Forchheimer extended Darcy model. Further, the local thermal non-equilibrium (LTNE) model is employed to express the heat transport phenomena within a porous medium. This work reveals the effects of the pertinent electromagnetic and thermophysical parameters on transport through a porous medium when exposed to an electromagnetic field. The following summarizes the conclusions arrived at in this work:

(1) The computational results are in excellent agreement with the results given by Amiri and Vafai [6]. This model can be used to describe the fundamental attributes of forced convection in a porous medium subject to an imposed electromagnetic field.
(2) Temperature and Nusselt number values increase substantially with an increase in the electromagnetic power.
(3) The existence of an optimum value for frequency in terms of attaining the maximum temperature within a porous medium has been established.
(4) Alterations of electromagnetic power and frequency have a prominent effect on the flow and temperature fields.
(5) An imposed electromagnetic field has a substantial effect in altering the local thermal equilibrium and dispersion effects within a porous medium.

Acknowledgement

The authors gratefully acknowledge the financial support for this work provided by the Thailand Research Fund (TRF).

References

[1] K. Vafai, M. Sozen, Analysis of energy and momentum transport for fluid flow through a porous bed, ASME J. Heat Transfer 112 (1990) 690–699.
[2] K. Vafai, M. Sozen, An investigation of a latent heat storage porous bed and condensing flow through it, ASME J. Heat Transfer 112 (1990) 1014–1022.
[3] M. Sozen, K. Vafai, Analysis of the non-thermal equilibrium condensing flow of a gas through a packed bed, Int. J. Heat Mass Transfer 33 (1990) 1247–1261.
[4] M. Quintard, S. Whitaker, One- and two-equation models for transient diffusion processes in two-phase systems, Adv. Heat Transfer 23 (1993) 369–464.
[5] M. Quintard, Modelling local thermal non-equilibrium heat transfer in porous media, in: Proceedings of the Eleventh International Heat Transfer Conference, vol. 1, 1998, pp. 279–285.
[6] A. Amiri, K. Vafai, Analysis of dispersion effects and non-thermal equilibrium, non-Darcian, variable porosity incompressible flow through porous media, Int. J. Heat Mass Transfer 37 (1994) 939–954.
[7] A.V. Kuznetzov, An analysis solution of heating a two-dimensional porous packed bed by a non-thermal equilibrium fluid flow, Appl. Sci. Res. 55 (1995) 83–93.
[8] A. Nakayama, F. Kuwahara, M. Sugiyama, G. Xu, A two-energy equation model for conduction and convection in porous media, Int. J. Heat Mass Transfer 44 (2001) 4375–4379.
[9] Pei-Xue Jiang, Ze-Pei Ren, Numerical investigation of forced convection heat transfer in porous media using a thermal non-equilibrium model, Int. J. Heat Fluid Flow 22 (2001) 102–110.
[10] Pei-Xue Jiang, Guang-Shu Si, Meng Li, Ze-Pei Ren, Experimental and numerical investigation of forced convection heat transfer of air in non-sintered porous media, Exp. Therm. Fluid Sci. 28 (2004) 545–555.
[11] S.M. Kuo, C.L. Tien, Transverse dispersion in packed sphere bed, in: Proceedings of the 25th ASME Heat Transfer Conference, Houston, Texas, 1988, pp. 629–634.
[12] C.T. Hsu, P. Cheng, Thermal dispersion in a porous medium, Int. J. Heat Mass Transfer 33 (1990) 1587–1597.

[13] M.L. Hunt, C.L. Tien, Non-Darcian flow, heat and mass transfer in catalytic packed-bed reactors, Chem. Eng. Sci. 45 (1990) 55–63.
[14] M. Sozen, K. Vafai, Longitudinal heat dispersion in porous media with real gas flow, J. Thermophys. Heat Transfer 7 (1993) 153–157.
[15] D.A. Nield, Effects of local thermal non-equilibrium in steady convection processes in a saturated porous medium: forced convection in a channel, J. Porous Media 1 (1998) 181–186.
[16] A.V. Kuznetsov, L. Cheng, M. Xiong, Effects of thermal dispersion and turbulence in forced convection in a composite parallel plate channel: investigation of constant wall heat flux and constant wall temperature cases, Numer. Heat Transfer A 42 (2002) 365–383.
[17] F. Kuwahara, A. Nakayama, Numerical determination of thermal dispersion coefficients using a periodic porous structure, J. Heat Transfer 121 (1999) 160–163.
[18] W. Bian, P. Vasseur, E. Bilgen, F. Meng, Effect of an electromagnetic field on natural convection in an inclined porous layer, Int. J. Heat Fluid Flow 17 (1996) 36–44.
[19] H. Ni, A.K. Datta, K.E. Torrance, Moisture transport in intensive microwave heating of biomaterials: porous media model, Int. J. Heat Mass Transfer 42 (1999) 1501–1512.
[20] P. Ratanadecho, K. Aoki, M. Akahori, Influence of irradiation time, particle sizes, and initial moisture content during microwave drying of multi-layered capillary porous materials, J. Heat Transfer 124 (1) (2002) 151–161.
[21] P. Rattanadecho, The simulation of microwave heating of wood using a rectangular wave guide: influence of frequency and sample size, Chem. Eng. Sci. 61 (2006) 4798–4811.
[22] P. Rattanedecho, N. Suwannapum, W. Cha-um, Interactions between electromagnetic and thermal fields in microwave heating of hardened type *I*-cement paste using a rectangular waveguide (influence of frequency and sample size), ASME J. Heat Transfer 131 (2009) 082101–082112.
[23] Ryoji Shigemitsu, Toshio Tahawa, Hiroyuki Ozoe, Numerical computation for natural convection of air in a cubic enclosure under combination of magnetizing and gravitational forces, Numer. Heat Transfer A 43 (5) (2003) 449–463.
[24] Q.W. Wang, M. Zeng, Z.P. Huang, G. Wang, H. Ozoe, Numerical investigation of natural convection in an inclined enclosure filled with porous medium under magnetic field, Int. J. Heat Mass Transfer 50 (2007) 3684–3689.
[25] D.D. Dinčov, K.A. Parrot, K.A. Pericleous, Heat and Mass transfer in two-phase porous materials under intensive microwave heating, J. Food Eng. 65 (2004) 403–412.
[26] T. Basak, A. Meenakshi, Influence of ceramic supports on microwave heating for composite dielectric food slabs, AIChE J. 52 (6) (2006) 1995–2007.
[27] W. Cha-um, W. Pakdee, P. Rattanadecho, Experimental analysis of microwave heating of dielectric materials using a rectangular wave guide (MODE: TE_{10}) (case study: water layer and saturated porous medium), Exp. Therm. Fluid Sci. 33 (3) (2009) 472–481.
[28] S.V. Patankar, Numerical Heat Transfer and Fluid Flow, Hemisphere/McGraw-Hill, New York, 1980.